View Journal

Dalton Transactions

Accepted Manuscript

This article can be cited before page numbers have been issued, to do this please use: M. D. C. Gimenez Lopez, M. Clemente Leon and C. Giménez-Saiz, *Dalton Trans.*, 2018, DOI: 10.1039/C8DT01269E.

ROYAL SOCIETY OF CHEMISTRY

rsc.li/dalton

View Article Online
DOI: 10.1039/C8DT01269E

Unravelling the spin-state of solvated $[Fe(bpp)_2]^{2+}$ spin-crossover complexes: structure-function relationship

Maria del Carmen Giménez-López[a],* Miguel Clemente-León[b], Carlos Giménez-Saiz[b].

[a]Centro Singular de Investigación en Química Biolóxica e Materiais Moleculares (CIQUS), Universidade de Santiago de Compostela, 15782 Santiago de Compostela, Spain. E-mail: Maria.Gimenez.Lopez@usc.es
[b]Instituto de Ciencia Molecular, Universidad de Valencia, P.O. Box 22085, 46071 Valencia, Spain

Abstract

This paper reports firstly the syntheses, crystal structures thermal and magnetic properties of spin crossover salts of formula $[Fe(bpp)_2]_3[Cr(CN)_6]_2 \cdot 13H_2O$ (**1**) and $[Fe(bpp)_2][N(CN)_2]_2 \cdot 1H_2O$ (**2**) (bpp = 2,6-bis(pyrazol-3-yl)pyridine) exhibiting hydrogen-bonded networks of low-spin $Fe(bpp)_2]^{2+}$ complexes and $[Cr(CN)_6]^{3-}$ or $[N(CN)_2]^-$ anions, with solvent molecules sitting in the voids. Desolvation of **1** is accompanied by a complete low-spin (LS) to a high-spin (HS) transformation that becomes reversible after rehydration by exposing the sample to the humidity of the air. The influence of the lattice water in the magnetic properties of spin-crossover $[Fe(bpp)_2]X_2$ complex salts has been documented. In most cases, it stabilises the LS sate over HS one. In other cases, it is rather the contrary. The second part of this paper is devoted to unravel the reasons why the lattice-solvent stabilise one form over the other through magneto-structural correlations of $[Fe(bpp)_2]^{2+}$ salts bearing anions with different charge/size ratio (X^{n-}). The $[Fe(bpp)_2]^{2+}$ stacking explaining these two different behaviours is correlated here with the composition of second coordination sphere of the Fe centers and the ability of these anions to form hydrogen bonds and/or π- π stacking interactions between them or the bpp ligand.

Introduction

Next-generation of high capacity memory devices,[1,2] multifunctional hybrid materials,[3] and other applications, including chemical and pressure sensors [4-7] could be based on switching magnetic materials such as Fe(II) spin-crossover (SCO) complexes.[8-15] The magnetic state of these bistable materials can be tuned from a low-spin configuration (LS, *S=0*) to a high-spin configuration (HS, *S=2*) through external stimuli: thermally, by means of light irradiation, or under pressure.[16-28] Attempts to electrically and mechanically stretching control the spin states on SCO complexes have been also reported. [29-30]

Bistability is undoubtedly one of the most desired properties when designing new technological materials. [31-33] One particular challenge for harnessing the magnetic bistability of these molecular switches is however the integration into functional nanostructures[20] such as nanoparticles, thin films or surface patterns, while controlling their functional properties.[34] In Fe SCO complexes there are many subtle factors determining the characteristics of the transition such as (i) the nature of the counter-ion when the SCO complexes are cationic, (ii) the existence of intermolecular interactions between the SCO complexes, and (iii) the presence/absence of solvates (that may interact with the SCO complexes modifying the ligand field or cause a pressure effect).[35-37] Understanding how these factors

View Article Online
DOI: 10.1039/C8DT01269E

control the thermal spin-transition in solvated crystals (from LS to HS, and *viceversa*) is highly desirable to design switchable nanostructure materials, with predictable properties, without attendant problems of deterioration of the SCO functionality during solvent processing and/or device fabrication. [38]

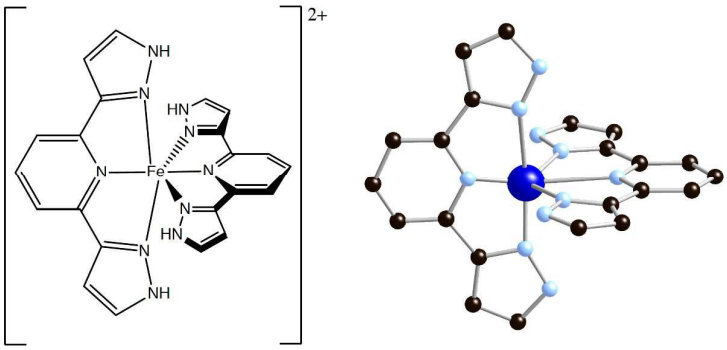

Figure 1. Schematic representation (on the left) and chemical structure (on the right) of the $Fe(bpp)_2]^{2+}$ complex with the tridentade bpp ligand binding to the metal ion in the meridional positions. Carbon, nitrogen and iron atoms are shown as black, light-blue and dark-blue circles, respectively. Hydrogen atoms have been omitted for clarity.

It is known that the magnetic properties of SCO complexes may depend on the presence of solvent or other guest-molecules in the crystal, which has been used for sensing applications.[39-41] For example, spin-transitions associated with the loss or gain of solvated molecules have been reported in $[Fe(bpp)_2]X_2$ complex salts (bpp = 2,6-bis(pyrazol-3-yl)pyridine; X = anion) (Figure **1**).[42,43] In these salts, the imine N atoms coordinates to the Fe^{2+} cation, whereas the presence of the amino groups (-N–H) ensures the formation of strong hydrogen bonds with solvent molecules and/or anions present in the solid.[44] The desolvated salts of these complexes are technologically very important, as they can exhibit intrinsic spin-crossover that takes place abruptly and with thermal hysteresis close to room temperature. The solvated species are generally diamagnetic, whereas the corresponding anhydrous compounds are found to be paramagnetic.[45] Thus, a conversion from the LS state to the HS state is often observed after the loss of solvated molecules. For salts of $[Fe(L)_n]^{2+}$ (L = ligand) cations whose ligand donor groups contain hydrogen-bond donors, it has been generally accepted that lattice-solvent stabilizes the LS form of the complex via hydrogen bonding (behaviour **A**). [46] This is the case for most of the $[Fe(bpp)_2]^{2+}$ complexes reported in the literature, but not for all of them.[47-53] In a few cases, the stabilization of the HS state has been observed for the solvated compounds (behaviour **B**). Although many efforts have been made to understand how the temperature and cooperativity of these spin-crossover systems are influenced by their structure [38, 54], surprisingly the reasons why the lattice-solvent stabilise one form over the other (LS is most commonly observed) still remain unknown.

Here, we report a detailed discussion of comprehensive structural data for a series of $[Fe(bpp)_2]^{2+}$ complexes (Table 1) showing for the first time that is possible to correlate these two magnetic behaviours (**A** and **B**) with different packing modes of

View Article Online
DOI: 10.1039/C8DT01269E

the $[Fe(bpp)_2]^{2+}$ cations in the crystal thanks to thorough accumulative magneto-structural experimental evidences. In addition, solvated crystals of $[Fe(bpp)_2]^{2+}$ with two new anions ($[Cr(CN)_6]^{3-}$ and $[N(CN)_2]^-$) showing behaviour **A** have been growth by careful diffusion of their components through a gel (tetramethoxysilane) to yield compounds **1** and **2**, respectively, that further test our hypothesis. The syntheses, thermal properties, structures and magnetic characterizations of these new compounds are also reported here.

Table 1. A complete list of solvated $[Fe(bpp)_2]_nX_2$ complexes salts discussed in this paper with different anions (X^{n-}) are presented in this table ($X^{n-} = ClO_4^-$, $[Cr(ox)_3]^{3-}$, $[Cr(CN)_6]^{3-}$, $[N(CN)_2]^-$, $[Hchtc]^{2-}$, $[Cu(pds)_2]^-$, $[Cr(bpy)(ox)_2]^-$ and $[Cr(phen)(ox)_2]^-$ where ox = oxalate, Hchtc = cis,cis-1,3,5-monoprotonated cyclohexanetricarboxylate, pds = pirazine-2,3-diselenolate, bpy = 2,2'-bipyridine and phen = 1,10-phenantroline). **8r** and **9r** have been obtained after rehydration of a dried sample of **8** and **9**, respectively.

Compound	Formula	Ref.
1	$[Fe(bpp)_2]_3[Cr(CN)_6]_2 \cdot 13H_2O$	This paper
2	$[Fe(bpp)_2][N(CN)_2]_2 \cdot H_2O$	This paper
3	$[Fe(bpp)_2]_2[Cr(ox)_3]ClO_4 \cdot 5H_2O$	43
4	$[Fe(bpp)_2][Cu(pds)_2] \cdot 2.5MeOH$	47
5	$[Fe(bpp)_2][Hchtc] \cdot 5.5H_2O$	48
6	$[Fe(bpp)_2][Cr(bpy)(ox)_2]ClO_4 \cdot EtOH \cdot 4H_2O$	49
7	$[Fe(bpp)_2][Cr(phen)(ox)_2]ClO_4 \cdot 1.5EtOH \cdot 4H_2O$	49
8	$[Fe(bpp)_2][Cr(bpy)(ox)_2]_2 \cdot 2H_2O$	50, 51
8r	$[Fe(bpp)_2][Cr(bpy)(ox)_2]_2 \cdot 2H_2O$	50, 51
9	$[Fe(bpp)_2][Cr(phen)(ox)_2]_2 \cdot 0.5H_2O \cdot 0.5MeOH$	51
9r	$[Fe(bpp)_2][Cr(phen)(ox)_2]_2 \cdot 0.5H_2O$	51
10	$[Fe(bpp)_2][Cr(phen)(ox)_2]_2 \cdot 5.5H_2O \cdot 2.5MeOH$	51

Experimental Section

Syntheses

All chemicals and solvents were used as received. The bpp ligand was synthesised according to previously described methods.[55,56]

View Article Online
DOI: 10.1039/C8DT01269E

Synthesis of $[Fe(bpp)_2]_3[Cr(CN)_6]_2 \cdot 13H_2O$ (1) and $[Fe(bpp)_2][N(CN)_2]_2 \cdot 1H_2O$ (2)
1 mL of tetrametoxisilano (TMS) [57] was added to a solution of $K_3[Cr(CN)_6]$ (0.015 g, 0.047 mmol) for **1** and $Na[N(CN)_2]$ (0.012 g, 0.140 mmol) for **2** in 9 mL of deionised water. The resulting mixture was homogenised by stirring and jellified in a thermostatised bath at 60 °C for 20 min. After cooling down the resulting gel, a solution of bpp (0.030g, 0.140 mmol) and $Fe(ClO_4)_2 \cdot 6H_2O$ (0.026g, 0.070 mmol) in 10 mL of ethanol solution (50%) was added in both cases. After a few days, large dark red crystals were obtained on the interface by slow diffusion.

For compound **1** Yield: 45%, 0.22 g. IR(KBr): ν = 3425 (vs, -O–H, water), {3138 (w), 3121 (w), 3093 (w)} (-N–H, bpp), {2923 (m), 2852 (m), 2738 (m)} (-C–H, bpp), 2129 (m, -C≡N, $[Cr(CN)_6]^{3-}$), 1629 (m, -O–H, water), 1617 (s, -C=C-, bpp), 1462-1277 (s, -C=N-, bpp), 1230-1000 (w, -C–H-, bpp), 773 (s, -C=C-, bpp), 458 (i, -Cr–CN-, $[Cr(CN)_6]^{3-}$) cm^{-1}. $C_{78}H_{80}Cr_2Fe_3N_{42}O_{13}$ (5134.53): calcd. C 44.93, H 3.86, N 28.21; found C 45.08, H 3.80, N 28.15; calcd Cr/Fe 40:60; found 39.6:60.4.

For compound **2**: Yield: 65%, 0.024 g. IR(KBr): ν = 3460 (w, -O–H, water), {3135 (w), 3127 (w), 3083 (w)} (-N–H, bpp), {2872 (m), 2791 (m), 2682 (m)} (-C–H, bpp), 2270-2150 (vs, -C≡N, $[N(CN)_2]^-$), 1615 (s, -C=C-, bpp), 1460-1275 (s, -C=N-, bpp), 1230-1000 (w, -C–H-, bpp), 767 (s, -C=C-, bpp), cm^{-1}. $C_{26}H_{20}Fe_1N_{10}O_1$ (544.35): calcd. C 57.37, H 3.70, N 25.73; found C 57.11, H 3.79, N 25.77.

Characterisation techniques
Direct current (dc) magnetic susceptibility measurements were carried out on polycrystalline samples with a Quantum Design MPMS-XL-5 magnetometer equipped with a SQUID sensor. Variable-temperature measurements were performed in the 2–400 K temperature range with an applied magnetic field of 0.1 T. The temperature sweeping rate for compound **1** and **2** was as follow: 0.5 K min^{-1} (2–60 K) and 1.5 K min^{-1} (60–400 K). Dehydrated samples of **1** were obtained *in situ* by maintaining the sample in the SQUID at 400 K for 120 min until a constant magnetic value was observed. Susceptibility data was corrected for the diamagnetic contribution of the salts using Pascal's constants.[58] Perforated plastic capsules were used to enable the loss of the solvated molecules.
Thermogravimetric analysis (TGA) measurements were carried out in a Mettler Toledo TGA/SDTA/851^e apparatus in the 298–413 K temperature range under a dry nitrogen atmosphere and at a scan rate of 1 K min^{-1}. The dehydration–rehydration process was monitored by heating grinded samples under a stream of nitrogen from 298 to 413 K (1 K min^{-1}). Then, the system was kept at this temperature for 20 min to allow complete loss of water molecules. Afterward, the sample was cooled to 298 K. At this point, the stream of nitrogen was replaced by a stream of humid air to allow complete rehydration of the samples. The total flux of nitrogen was constant during the experiment.
IR transmission measurements of KBr pellets were recorded at room temperature with a Nicolet Avatar 320 FT-IR spectrophotometer in the range 4000–400 cm^{-1}.
CHN elemental analyses were carried out in a CE instrument EA 1110CHNS analyzer. The expected Cr:Fe ratio was confirmed on a Philips ESEM X230 scanning electron microscope equipped with an EDAX DX–4 microsonde.

View Article Online
DOI: 10.1039/C8DT01269E

Differential scanning calorimetry measurements under nitrogen atmosphere were performed in a Mettler Toledo DSC/821^e apparatus with warming and cooling rates equal to 4 K min^{-1}. A correction from the sample holder was automatically applied.

Crystal structure determination

Suitable crystals of **1** and **2** were coated with oil, suspended on small fiber loops and placed in a stream of cold nitrogen.

Crystal data for **1:** $C_{78}H_{80}Cr_2Fe_3N_{42}O_{13}$, M = 2085.39, crystal dimensions: 0.34 × 0.11 × 0.09 mm, monoclinic, *C 2/c*, a = 18.4284(3), b = 24.2368(5), c = 23.7068(4) Å, α= 90.000(0), β = 110.9946(11), γ = 90.000(0), V = 9885.6(3) Å^3, Z = 4. A dark-red prismatic single crystal of **2** was used for data collection at room temperature with a Nonius KappaCCD diffractometer using a graphite monochromated Mo-K_α radiation source (λ = 0.71073 Å). Denzo and Scalepack[59] programs were used for cell refinements and data reduction. The structure was solved by direct methods using the SIR97[60] program with the WinGX[61] graphical user interface. The structure refinements were carried out with SHELX–2016/4.[62] Multiscan absorption corrections, based on equivalent reflections were applied to the data using the program SORTAV.[63] Of 20878 collected reflections, 11318 (2.9°< 2θ < 55°) were independent (R_{int} = 0.0515) and used to refine 642 parameters and 6 restraints. All non-hydrogen atoms were refined anisotropically, except some oxygen atoms belonging to disordered water molecules having partial occupancy factors. H atoms of –NH groups were found in difference maps and refined positionally with geometric restraints. H atoms on carbon atoms were placed in calculated positions and refined with a riding model. H atoms of water molecules were not found. Final R [I > 2σ (I)]: R_1 = 0.0530, wR_2 = 0.1551; final R (all data): R_1 = 0.1135, wR_2 = 0.1825. Max./ min. residual peaks in the final difference map: 0.751/–0.307 e·Å^{-3}.

Crystal data for **2:** $C_{26}H_{18}Fe_1N_{10}O_1$, M = 542.33, crystal dimensions: 0.22×0.18×0.12 mm, monoclinic, *C 2/c*, a = 11.8050(6), b = 19.8640(10), c = 11.8430(7) Å, α = 90.000(0), β = 90.2620(20), γ = 90.000(0), V = 2777.1(3) Å^3, Z = 2, $\rho_{calcd.}$ = 1.479 M·m^{-3}, μ*(Mo-Kα)* = 0.595 mm^{-1}. A dark-red plate-like single crystal of **3** was used for data collection at 293(2) K with a Stoe Imaging Plate Diffractometer System (IPDS) diffractometer equipped with a graphite-monochromated Mo-K$_\alpha$ radiation source (λ = 0.71073 Å), and an Oxford Cryostream Cooler Device. Data were collected using the φ rotation movement with a crystal-to-detector distance of 70 mm (φ = 0.0–250°, Δφ = 1.4°). Of 2840 measured reflections, 1535 (2.01°< 2θ < 26.35°) were independent (R_{int} t = 0.0806) and used to refine 202 parameters. The structure was solved by direct methods (SIR97) [60] and refined against F^2 with a full- matrix least-squares algorithm using SHELXL-97[62] and the WinGX (1.64) software package.[61] All non-hydrogen atoms were refined anisotropically. H-atoms were added in calculated positions and refined riding on the corresponding atoms except H atoms of –NH groups and water molecules. H-atoms of –NH groups were located by difference Fourier maps and refined isotropically. Final R [I > 2σ(I)]: R_1 = 0.0807, wR_2 = 0.1883; final R (all data): R_1 = 0.1722, wR_2 = 0.2577. Max./ min. residual peaks in the final difference map: 1.060/–1.096 e·Å^{-3}.

CCDC-962306 for **1** and CCDC-1435556 for **2** contain the supplementary crystallographic data for this paper. These data can be obtained free of charge from

View Article Online
DOI: 10.1039/C8DT01269E

The Cambridge Crystallographic Data Centre via www.ccdc.cam.ac.uk/data_request/cif.

Results and discussion

Synthesis, crystal structure and thermal properties of 2 and 3.

Crystals of **1** and **2** were only obtained after slow diffusion of an ethanolic solution of $[Fe(bpp)_2](ClO_4)_2$ through a gel formed by hydrolysis and polycondensation of tetramethoxysilane containing $K_3[Cr(CN)_6]$ and $Na[N(CN)_2]$, respectively. It is worth noting that the direct reaction of the precursors under stoichiometric conditions led to the fast precipitation of the compounds as fine powders.

1 crystallises in the monoclinic space group *C 2/c*. Its structure comprises isolated $[Fe(bpp)_2]^{2+}$ and $[Cr(CN)_6]^{3-}$ complex ions together with water molecules. The crystal structure contains two inequivalent Fe^{2+} sites (Fe(1) and Fe(2)). The Fe–N bond lengths found in the range 1.911(3)–1.985(3) Å are typical of the LS configuration that is the usual stable spin state in hydrated $[Fe(bpp)_2]X_2$ salts.[64] Both centers adopt a slightly distorted C_{2v} symmetry, with the tridentate bpp ligand binding to the metal ion in meridional positions. The values observed for the ε (□□□□□□ 110.5(4)-110.4(4)º, □□□2□□ 110.4(4)-110.8(4)º) and δ angles (□□□□□□ 114.6(4)-114.8(4)º, □□□2□□ 113.7(4)-114.6(3)º) of the chelate ring are similar to those found in $[Fe(bpp)_2]^{2+}$ LS complexes. The second coordination sphere of both Fe centers is occupied by two $[Cr(CN)_6]^{3-}$ anions and two water molecules. However, due to the local symmetry of the Fe(1) (C_2), one of the bpp ligands is hydrogen-bonded through its non-coordinated NH groups to two $[Cr(CN)_6]^{3-}$ anions, whereas the other bpp ligand is connected through hydrogen bonding to two water molecules (Figure **2a**). In the Fe(2) site, each bpp ligand is hydrogen-bonded to one $[Cr(CN)_6]^{3-}$ anion and one water molecule (Figure **2b**).

The crystal packing of **1** is best described as composed of layers of $[Fe(bpp)_2]^{2+}$ cations and $[Cr(CN)_6]^{3-}$ anions that alternate along the *y* direction with water molecules forming a complex hydrogen-bonding network involving the non-coordinated NH groups of the $[Fe(bpp)_2]^{2+}$ and the –CN groups of the $[Cr(CN)_6]^{3-}$ anions (Figure **3a**). In the cationic layer, each $[Fe(bpp)_2]^{2+}$ complex interact via π– π stacking with four neighbouring iron complexes, giving rise to the terpyridine embrace motif (Figure **3b**). Within the cationic layer, the two crystallographically independent Fe^{2+} sites (Fe(1) and Fe(2), depicted in yellow and blue, respectively) form stacks (…Fe(2)Fe(2) Fe(1)…) along the z axis with the shortest distance between Fe^{2+} sites of 7.833(3) Å (Fe(1) ···Fe(2)), whereas the shortest distance between Fe^{2+} sites in adjacent layers is 11.230(3) Å. The study of the crystal packing of the iron complexes across the third dimension reveals that consecutive layers are shifted with respect each other along the *x* direction, giving rise to a packing of the type AA'AA'.

View Article Online
DOI: 10.1039/C8DT01269E

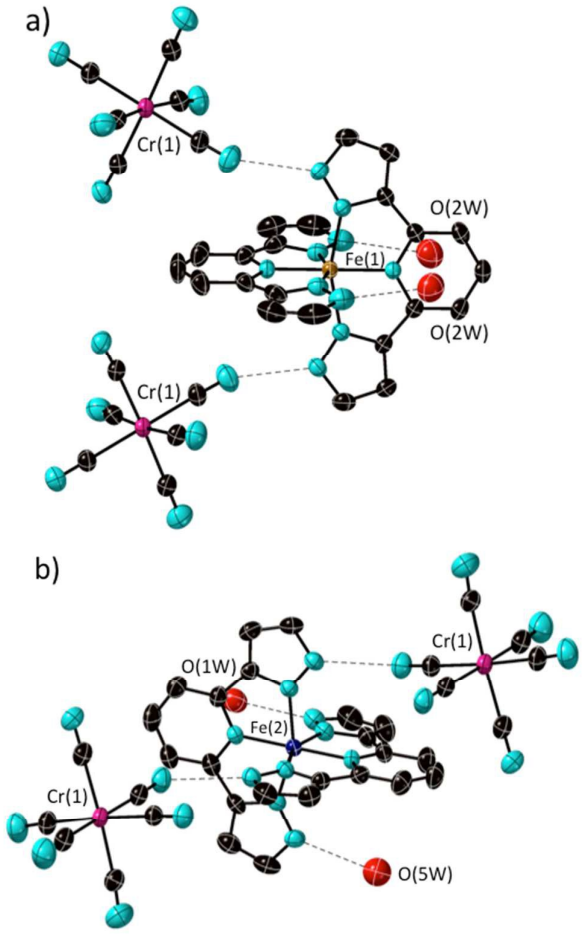

Figure 2. Thermal ellipsoid diagram of the crystal structure of the hydrated salt $[Fe(bpp)_2]_3[Cr(CN)_6]_2 \cdot 13H_2O$ (**1**) showing the first and second coordination spheres for the two crystallographic independent Fe^{2+} cations, Fe(1) (a) and Fe(2) (b). Carbon and nitrogen atoms are shown as black and light-blue, respectively. H atoms are omitted for clarity.

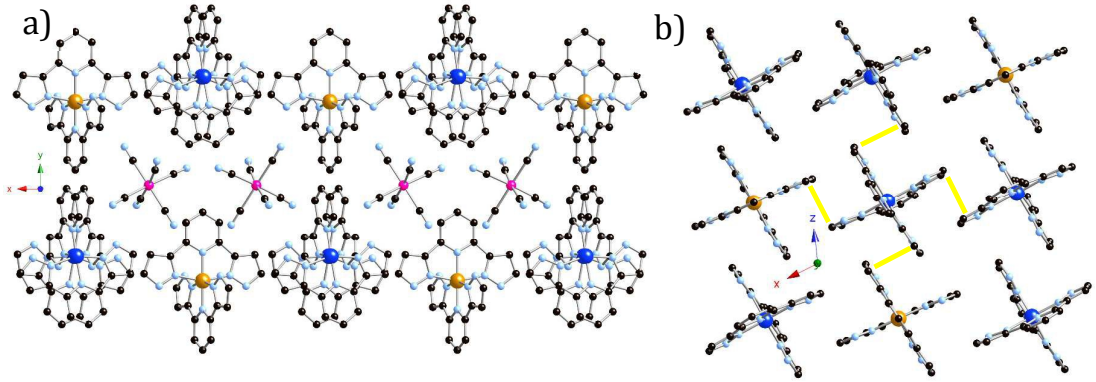

Figure 3. A projection of the crystal structure of **1** showing (a) alternating cationic and anionic layers onto the *xy* plane and (b) the arrangement of $[Fe(bpp)_2]^{2+}$ units onto the *xz* plane (yellow lines refer to π– π□□□□□□actions). Water molecules are omitted for clarity. Color code as it is indicated in Figure **2**.

View Article Online
DOI: 10.1039/C8DT01269E

Compound **2** also crystallises in the monoclinic space group *C 2/c*, and as in the case of compound **1**, its structure comprises isolated $[Fe(bpp)_2]^{2+}$ and $[N(CN)_2]^-$ complex ions together with a water molecule. In contrast to **1**, the structure of **2** contains only one independent Fe^{2+} site, with Fe–N distances in the range 1.96(6)–1.967(5) Å, characteristic of a LS configuration. The values observed for the ε (110.1(3)-110.5(4)º) and δ angles (114.5(3)-114.8(7)º) are those expected for a LS configuration. The second coordination sphere of the Fe^{2+} site is occupied by four $[N(CN)_2]^-$ anions (Figure **S1**). As in **1**, the crystal packing of **2** is best described as composed of layers of $[Fe(bpp)_2]^{2+}$ cations and $[N(CN)_2]^-$ anions that alternate along the *y* direction (Figure **S2**), being the shortest distance between Fe^{2+} sites in adjacent layers of 11.506(5) Å. Within the cationic layer, each $[Fe(bpp)_2]^{2+}$ complex (shortest distance between Fe^{2+} sites of 8.3803(6) Å) interact via π– π stacking with its four neighbouring iron complexes forming the typical terpyridine embrace motif (Figure **S2**).

In order to investigate the best temperature range for solvatomagnetism experiments, TGA analyses of **1** and **2** were performed. In compound **1** the loss of water molecules takes place in two separate temperature ranges (Figure **S3**). A progressively weight loss of ca. 3.5% between room temperature and 363 K corresponding to approximately to $4H_2O$ is first observed, while a much more abrupt weight loss (8.5%, corresponding to 7 H_2O molecules) takes place at higher temperatures (in the 363–408 K), suggesting the presence of stronger forces holding those water molecules in the structure by hydrogen bonding. In the case of **2**, a very small progressive weight loss of ca. 3% is observed below 363K **(**Figure **S4).** These results are in agreement with the formulation deducted from elemental analysis and X-ray crystal structure determinations (see below) and confirm that the involved desolvation are accessible within the temperature range of the magnetic measurements. Dehydratation–rehydratation studies for **1** show that when the anhydrous compound is exposed to the open air, more than half of the water molecules eliminated are readily recovered in just few minutes (62% weigh gain, corresponding to $8.5H_2O$) **(**Figure **4a)**. The sample undergoes several consecutive dehydratation–rehydratation experiments without apparent degradation.

Differential scanning calorimetry (DSC) measurements of **1** are consistent with the thermogravimetry data, as several endothermic peaks can be observed **(**Figure **4b**, curve 1). The first one that starts at 321 K with a high-temperature tail is in agreement with the gradual character of the first dehydration process. The second sharper peak centered at 379 K with a shoulder at 393K suggests that the second dehydratation process could take place with a subsequent spin change (from LS to HS, as discussed below) during the first cycle. The estimated enthalpy (ΔH) and enthopy (ΔS) values are as follow -176.0 $KJmol^{-1}$ and -469.6 $Jmol^{-1}K^{-1}$. Upon cooling to room temperature, a featureless curve is obtained, suggesting that the spin state of the Fe(II) complex remains unchanged in the temperature range studied. In the case of **2**, featureless calorimetric curves both on heating and cooling mode are observed in the temperature range studied indicating the absence of a thermally induced transition (Figure **S4**, curve 1). This is also in agreement with the very gradual and small weight loss observed in the TGA data below 363K.

View Article Online
DOI: 10.1039/C8DT01269E

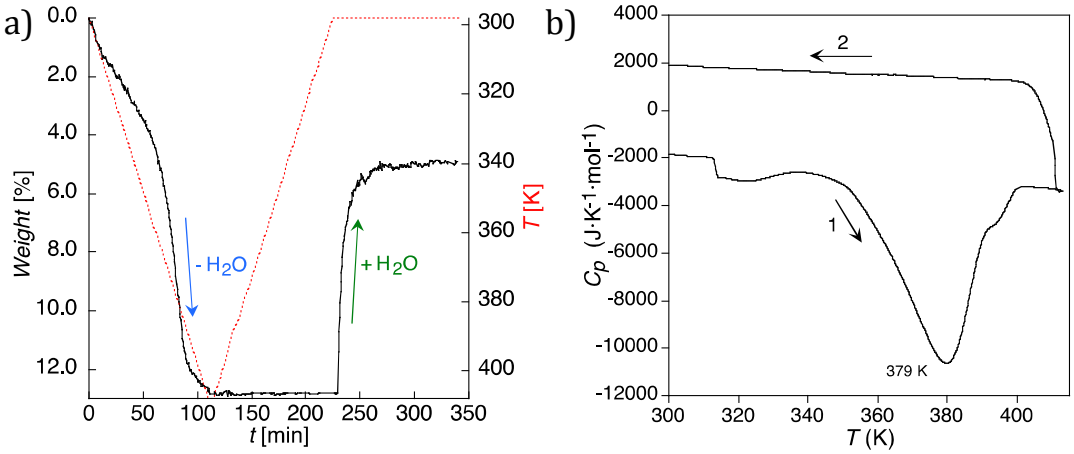

Figure 4. (a) TGA showing the dehydration–rehydration process (changes in temperature with the time during the experiment are shown by discontinue red line) and (b) DSC (curve 1: original sample in the heating mode, curve 2: subsequent temperature cycle in the cooling mode) of compound **1**.

Magnetic properties of 1 and 2

The temperature dependence of the $\chi_m T$ product (χ_m: molar magnetic susceptibility; T: absolute temperature) of **1** and its rehydrated sample (**1r**) are shown in Figure **5**. Both samples are exhibiting similar magnetic behaviour. In the first heating cycle (2–400K), the $\chi_m T$ is shown to be practically constant between 10 to 300 K with a value of 3.8 emuKmol^{-1} for **1** and 4.0 emuKmol^{-1} for **1r** at 300K. These values are in agreement with the "spin-only" value (χT=*3.75* emuKmol^{-1}) calculated for three Fe(II) in LS (t^6_{2g}, S=0) and two Cr(III) (t^3_{2g}, S=3/2) per formula. Above 350K, $\chi_m T$ for **1** starts to increase abruptly and reaches a value of 13.0 emuKmol^{-1} at 400K. For **1r**, the increase in $\chi_m T$ takes place practically at the same temperature and reaches a value of 12.1 emuKmol^{-1} at 400K. The $\chi_m T$ value observed for the hydrated sample is close with the value expected ($\chi_m T$ =*3.75* emuKmol^{-1}) for three Fe(II) in HS (t^4_{2g} e^2_g, S=2) and two Cr(III) (t^3_{2g}, S=3/2) per formula, whereas the value of the dehydrated sample is slightly lower. TGA and DSC studies confirm that the abrupt increase of $\chi_m T$ observed between 350–400K is due to a change of spin (from LS to HS) concomitant with the dehydration. As expected, the loss of the water molecules creates a negative pressure and the structure expands by populating the high spin state that is entropically favoured and then stabilised at high temperature since it has higher electronic degeneracy and larger density of vibrational states. Upon cooling, the $\chi_m T$ value decreases continuously until 50K reaching a value of 8.3 emuKmol^{-1} for **1** and 8.0 emuKmol^{-1} for **1r.** Below this temperature, both samples exhibit a more drastic decrease of $\chi_m T$ with decreasing temperature that can be attributed to zero-field splitting and spin-orbit coupling effects, although intermolecular interactions between the different pin carriers cannot be discarded. Successive temperature cycles (on heating and cooling mode that have been omitted for simplicity) show the same magnetic behaviour of the dehydrated phases for both

View Article Online
DOI: 10.1039/C8DT01269E

samples **1** and **1r**. Thus, the change in the $\chi_m T$ value observed between 50–400K could be due to a gradual spin transition of part of the Fe(II) centers.

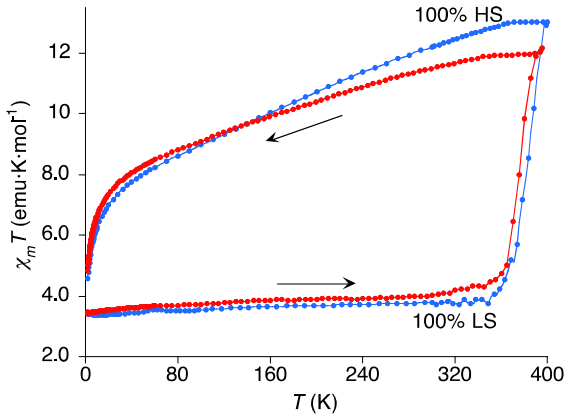

Figure 5. Temperature dependence of $\chi_m T$ in the temperature range between 2–400K on heating and cooling mode for **1** and the rehydrated sample (**1r**).

The thermal variation of $\chi_m T$ of **2** is shown in Figure **S5**. The first measurement performed on heating mode from 2K up to 350K shows a typical diamagnetic LS Fe(II) complex. At higher temperatures, dehydration starts and a small increase in the magnetic signal is observed upon heating. However, saturation of this signal is not observed (even after 2 h at 400 K, the maximum temperature available in our SQUID equipment). The spin transition of the anhydrous salt seems to occur at higher temperatures compare to that observed in compound **1**, where the separation distances between $[Fe(bpp)_2]^{2+}$ within the cationic layer are found to be smaller. It is worth noting that in this case the only solvated water molecule in the structure is not hydrogen-bonded to the non-coordinating N–H groups of the $[Fe(bpp)_2]^{2+}$ cations. As in the case of **1**, after rehydration the sample recovers the magnetic behaviour of the original sample.

Factors triggering the stabilisation of the LS form over the HS one, and *vice versa*, in solvated $[Fe(bpp)_2]^{2+}$ complexes

$[Fe(bpp)_2]^{2+}$ salts bearing anions with different charge/size ratio (X^{n-}, Figure **6**) where selected here to unravel this mystery, including those in compound **1** and **2**. It is interesting to note the ability of these anions to form hydrogen bonds and/or π- π stacking interactions between them or the bpp ligand. When solvated crystals of $[Fe(bpp)_2]^{2+}$ where obtained with anions exhibiting high charge/size ratio (compounds **1**, **2** and **3**), the LS state form was the stable phase (behaviour **A**) (Figure **7**, **S6** and **S7**). We believe that this is the case only for those SCO compounds with a "terpyridine embrace" lattice version, in which the $[Fe(bpp)_2]^{2+}$ cations are packed into two-dimensional (2D) layers interdigitated through face-to-face and edge-to-edge π- π□□□□□□□□□□□□□□ between the pyrazolyl groups on neighbouring molecules (3.187(8)–3.691(6) Å for **1** and 3.400(1)–3.763(3) Å for **2** and 3.202(4)–3.445(6) Å for **3**).[54] In fact, this is what we observe for most of the $[Fe(bpp)_2]^{2+}$ complexes reported in the literature with discrete anions (i.e. BF_4^-, ClO_4^-, PF_6^-, Br^-)[42,44,45] sandwiched by two adjacent $[Fe(bpp)_2]^{2+}$ layers interacting via van der Waals forces. Here, every bpp ligand exhibits aryl-aryl interactions with bpp ligands

View Article Online
DOI: 10.1039/C8DT01269E

of two different neighbour $[Fe(bpp)_2]^{2+}$ units (Fe···Fe distance within the same layer is 7.838(6) Å for **1**, 8.342(3) Å for **2** and 8.185(5) Å for **3**,), which triggers the stabilization of the LS state. Any perturbation of the intermolecular forces in the crystal will cause the stabilization of the HS (behaviour **B**), instead. Thus, when the anion size increases moderately, the separation between $[Fe(bpp)_2]^{2+}$ units within the 2D layer increases while their orientations remain unchanged. As a consequence, the number of aryl-aryl interactions drops and the stable form is now the HS state. This is what we saw for **4**, in which isolated $[Fe(bpp)_2]^{2+}$ units with none aryl-aryl interactions (Fe···Fe distance of 11.0701(2) Å) are found (Figure **S8**).[48] Similar effect has been observed recently for the methyl substituents of the bpp preventing the direct π- π□□□□□□□□□□between the pyrazole groups.[65] In other words, the terpyridine embrace motif is not longer favoured for larger anions or with a lower charge/radius ratio. We found that after the loss of the solvated molecules at 400 K the conversion from the LS state to the HS state is completed only for **1** and **3** (100 % HS), but no for **2**. The fact that in the later compound the solvated water molecule is not hydrogen-bonded to the non-coordinating N–H groups of the $[Fe(bpp)_2]^{2+}$ cations, in contrast with what is found for **1** and **3**, could explain the observed partial spin conversion.

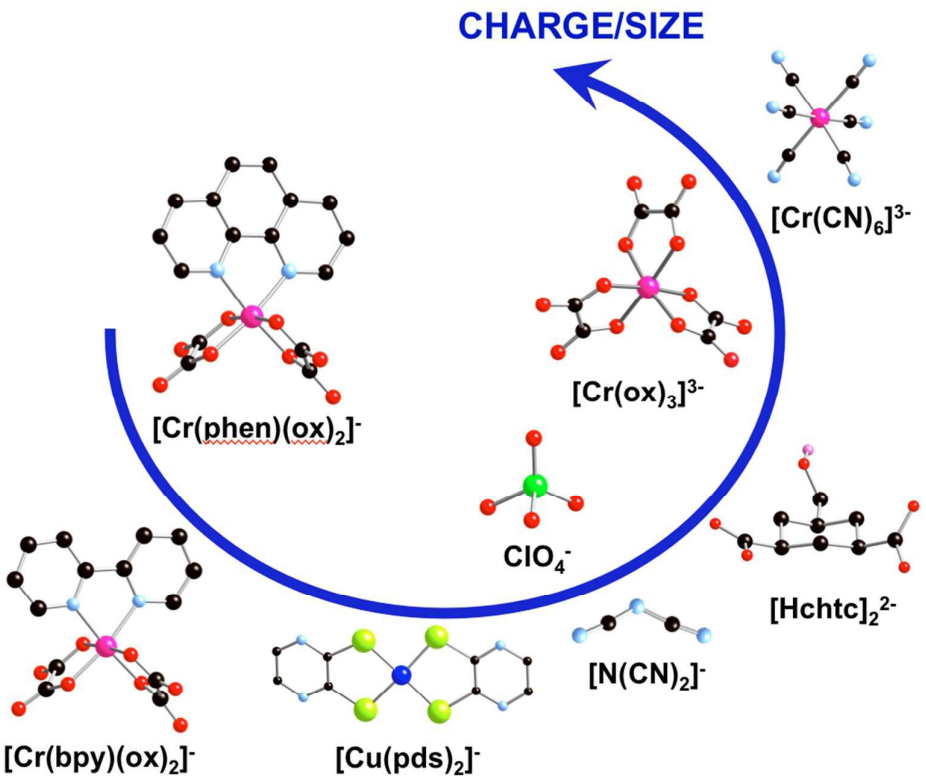

Figure 6. Charge/size ratio of the selected anions (X^{n-}) to form $[Fe(bpp)_2]^{2+}$ complexes. Carbon, nitrogen, oxygen, chlorine, chromium and selenium atoms are shown as black, light-blue, red, green, pink and dark-blue, respectively. H atoms are omitted for clarity.

View Article Online
DOI: 10.1039/C8DT01269E

On the contrary, when $[Fe(bpp)_2]^{2+}$ crystallises with bulky anions that show much lower charge/size ratio and high ability to establish π-π□stacking □□□□□□□□□□□□ (compounds **5**-**9**, **8r** and **9r**), we observe that the stable spin state form of the respectively solvated compound depends strictly on the composition of the second coordination sphere of $[Fe(bpp)_2]^{2+}$ (Figure **8** and S**9**). It is worth to note that $[Hchtc]_2^{4-}$ supramolecular synthons are found in the crystal structure of **5** (Figure S**10**). Thus, when the four non-coordinating N–H groups of $[Fe(bpp)_2]^{2+}$ are hydrogen-bonded to four $[Cr(L)(ox)_2]^-$ anions, the Fe–N bond lengths found are typical of LS values (1.914(6)–2.013(7) Å for **9r**) and the behaviour observed is always **A**. However, when three or two of the four non-coordinating N–H groups of $[Fe(bpp)_2]^{2+}$ are hydrogen-bonded to $[Cr(L)(ox)_2]^-$ anions and the rest of non-coordinating N–H groups to solvent molecules, the behaviour observed is **B** and the Fe–N distances found are characteristic of the HS configuration (2.130(2)–2.214(2) Å for **5**, 2.118(3)–2.223(3) Å for **6**, 2.130(4)–2.223(4) Å for **7** and 2.145(3)–2.204(3) Å for **8r**). Since the oxalate oxygen atom of the anion is a better hydrogen acceptor than the oxygen from the solvent molecule (water or methanol), it is expected an increase of the electron density of the non-coordinating nitrogen for the $[Fe(bpp)_2]^{2+}$ complex surrounded by four anions with respect to the complex surrounded by solvated molecules and anions. This leads to stronger donor–metal σ-interaction, and therefore, to shorter N(imine)–Fe σ bond favouring the LS state for the $[Fe(bpp)_2]^{2+}$ complex surrounded only by anions. However, when one of the N–H groups is connected to a Cr-bonded O atom, the solvated compound (**10**) shows a HS state for the Fe^{2+} center because metal-bonded O atoms are poorer hydrogen-bond acceptors than the terminal ones. For those compounds (**8** and **9**) where LS and HS Fe^{2+} centers coexist in the same crystalline phase (Fe_{HS}–N distances: 2.146(2)-2.210(2) Å for **8** and 2.159(2)-2.229(2) Å for **9**; Fe_{LS}–N distances: 1.921(2)-1.976(2) Å for **8** and 1.924(2)-1.985(2) Å for **9)**, the compositions of their second coordination spheres are consistent with the mentioned tendencies. This is in sharp contrast with our observations for **1** and **3** where crystallographically independent Fe^{2+} sites with mixed second coordination spheres containing solvent molecules and anions show a LS configuration (behaviour **A**) ((Fe_1–N: 1.919(5)-1.985(3) Å and Fe_2–N: 1.911(3)-1.985(3) Å for **1**; Fe_1–N: 1.934(7)-2.002(8) Å and Fe_2–N: 1.901(6)-1.985(7) Å for **3**;)) (Figure **2** and **S11**).

View Article Online
DOI: 10.1039/C8DT01269E

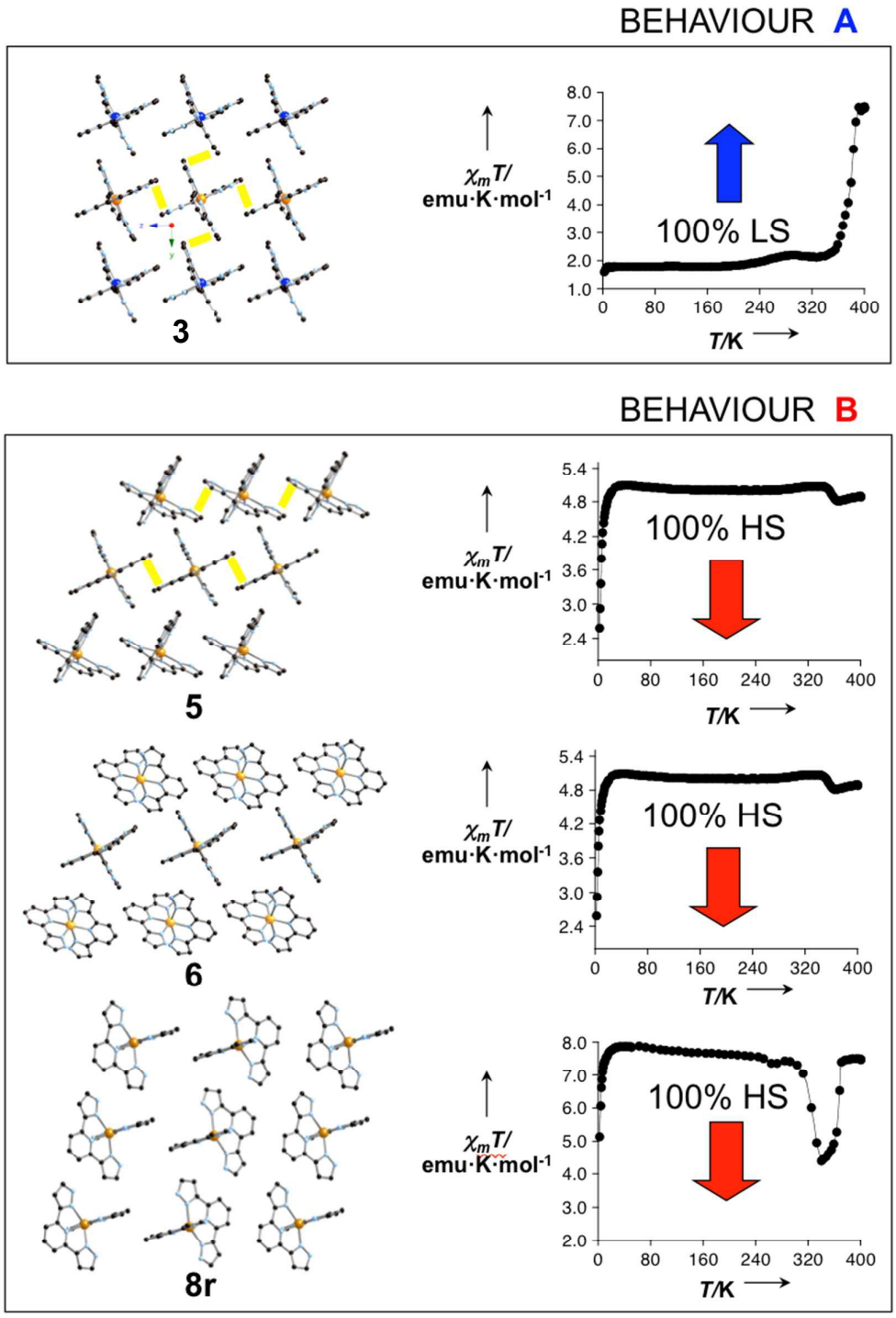

Figure 7. Magneto-structural correlations for **3**, **5**, **6**, and **8r** showing the relationship between the different packing diagrams found in a 2D single layer for the $[Fe(bpp)_2]^{2+}$ SCO units and the variable-temperature magnetic susceptibility (2–400 K) towards the desolvation process that define behaviour **A** and **B**. $\chi_m T$ values shown here are per formula (one Fe(II) centre in **5**, **6** and **8,** and two Fe(II) centres in **3**). π-π□stacking □□□□□□□□□□□□ between bpp ligands of neighbour $[Fe(bpp)_2]^{2+}$ units are shown in yellow. Iron atoms are shown in yellow or blue. Carbon and

View Article Online
DOI: 10.1039/C8DT01269E

nitrogen atoms are shown as black, and light-blue, respectively. H atoms are omitted for clarity.

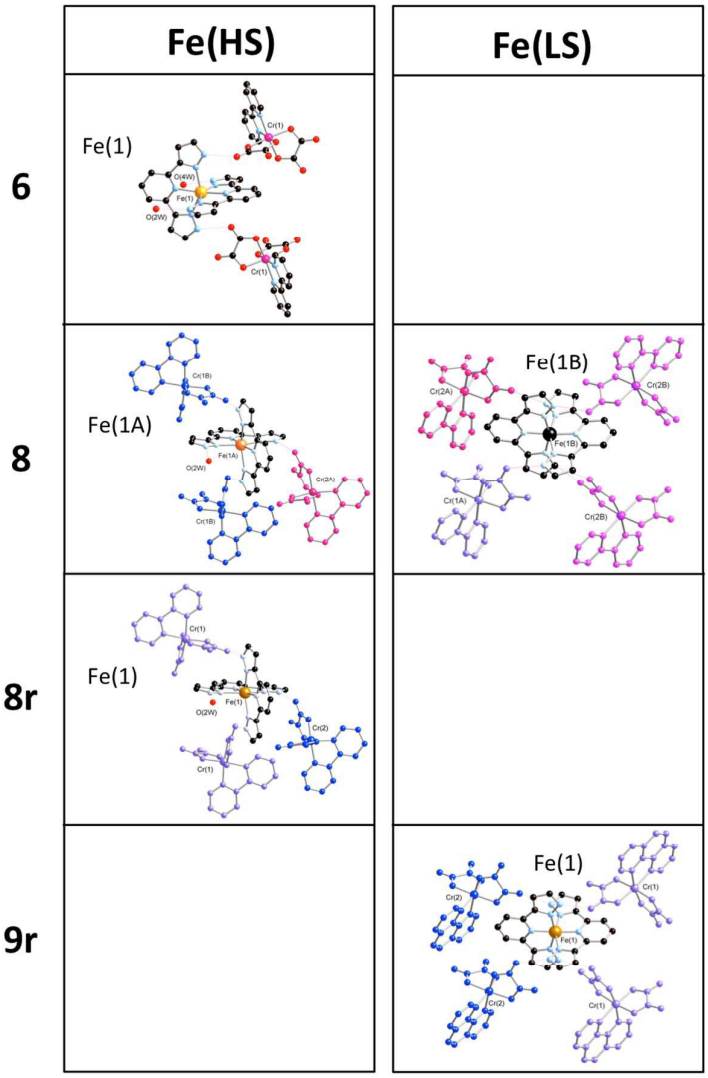

Figure 8. Composition of the second coordination sphere of the HS and LS Fe^{2+} centers for **6-9**, **8r** and **9r**. The same color has been used for all the atoms for the same crystallographic anion for the sake of clarity.

Strikingly, the packing of $[Fe(bpp)_2]^{2+}$ SCO complexes for any of the mentioned compounds (**5-9**, **8r** and **9r**) in which the composition of the second coordination sphere seems to play a crucial role does not show the typical "terpyridine embrace" lattice, as the relative orientation of the $[Fe(bpp)_2]^{2+}$ units have changed within the 2D layer (Figure **7** and **S12-S16**). We observed that the number of aryl-aryl interactions between the $[Fe(bpp)_2]^{2+}$ units decreases with the ability of the anions to form π-π□stacking interactions (Figure **S17-S18**). Whereas for **8** and **9** the $[Fe(bpp)_2]^{2+}$

View Article Online
DOI: 10.1039/C8DT01269E

cations are organized into dimers by π- π stacking interactions (3.203(3) Å for **8** and 3.273(2)–3.490(4) Å for **9**) (Figure **S19**), the zigzag arrangement observed for **6** and **7** (Figure **7** and **S12**) excludes the possibility of any stacking interaction between the SCO units. For the rehydrated compounds (**8r** and **9r**), where the extension of the hydrogen-bonding network has decreased with respect to the initial samples, the same tendency for the composition of the second coordination sphere of the Fe^{2+} center is observed. It is worth noting that for anhydrous crystals of $[Fe(bpp)_2]^{2+}$ with nitropusside that does not show the typical "terpyridine embrace" lattice, a LS configuration is also found when all the non-coordinating N–H groups are hydrogen-bonded to anions.[66]

Conclusions

Hydrogen-bonded assemblies of $[Fe(bpp)_2]^{2+}$ cations, and $[Cr(CN)_6]^{3-}$ or $[N(CN)_2]^-$ anions exhibiting spin crossover after dehydration have been obtained. The process is reversible as the rehydrated samples showed the same magnetic behaviour as the initial ones due to the lattice-solvent stabilisation of the LS configuration. We have clearly revealed the reasons for the two different behaviours of the solvated $[Fe(bpp)_2]^{2+}$ spin-crossover complexes bearing anions with different charge/size ratio (X^{n-}). When a "terpyridine embrace" lattice version is found, a conversion from the LS state to the HS state is observed after the loss of solvated molecules (behaviour **A**). However, when the $[Fe(bpp)_2]^{2+}$ complexes do not show π- π stacking interactions with neighbouring SCO complexes, the composition of the second coordination sphere of the $[Fe(bpp)_2]^{2+}$ complexes determines the spin state of the solvated SCO compounds, and therefore, the behaviour observed towards the desolvation (**A** or **B**). We can now rationalise and predict the spin state behaviour of $[Fe(bpp)_2]^{2+}$ spin-crossover complexes towards the loss of solvated molecules, after the thorough analysis of the magneto-structural correlations for more than twelve crystals. These findings will enable and facilitate the addressability and integration of SCO compounds into functional nanostructures preserving and improving their SCO functionality.

Conflicts of interest

There are no conflicts of interest to declare.

Acknowledgements

The authors acknowledge the Royal Society (DH110080 fellowship for M.C.G-L.), the European Research Council (ERC StG-679124 for M.C.G-L.) and the Generalitat Valenciana for funding this work, and J. M. Martinez-Agudo for technical assisstance with the acquisition of magnetic and DSC data.

References:

View Article Online
DOI: 10.1039/C8DT01269E

[1] O. Kahn, C. Jay Martinez, *Science* **1998**, 279, 44–48.
[2] O. Kahn, J. Krober, C. Jay Martinez, *Adv. Mater.* **1992**, 4, 718–728.
[3] A. B. Gaspar, V. Ksenofontov, M. Seredyuk, P. Gütlich, *Coord. Chem. Rev.* **2005**, 249, 2661–2676.
[4] R. N. Muller, L. Vander Elst, S. Laurent, *J. Am. Chem. Soc.* **2003**, 125, 8405–8407.
[5] Topics In Current Chemistry, ed. P. Gütlich and H. A. Goodwin, Springer Verlag, Berlin–Heidelberg–New York, **2004**, 233–235.
[6] A. D. Naik, K. Robeyns, C. F. Meunier, A. F. Leonard, A. Rotaru, B. Tinant, Y. Filinchuk, B. L. Su, Y. Garcia, *Inorg. Chem.*, **2014**, 53, 1263–1265.
[7] C. Bartual-Murgui, A. Akou, C. Thibault, G. Molnar, C. Vieu, L. Salmon, A. Bousseksou, J. Mater. Chem. C, **2015**, 3, 1277–1285.
[8] P. Gütlich, A. Hauser, H. Spiering, *Angew. Chem. Int. Ed. Engl.* **1994**, 33, 2024–2054.
[9] K. S. Kumar, I. Šalitroš, B. Heinrich, O. Fuhr , M. Ruben. *J. Mater. Chem. C*, **2015**, 3, 11635–11644.
[10] B. Schäfer, C. Rajnák, I. Šalitroš, O. Fuhr, D. Klar,C. Schmitz-Antoniak, E. Weschke, H. Wende, M. Ruben, *Chem. Commun.*, **2013**, 49, 10986.
[11] E. J. Devid, P. N. Martinho, M. V. Kamalakar, I. Šalitroš, Ú. Prendergast, J.-F. Dayen, V. Meded, T. Lemma, R. González-Prieto, F. Evers, T. E. Keyes, M. Ruben, B. Doudin and S. J. van der Molen, *ACS Nano*, **2015**, 9, 4496–4507.
[12] G. Molnár, L. Salmon, W. Nicolazzi, F. Terki, A. Bousseksou, *J. Mater. Chem. C*, **2014**, 2, 1360–1366.
[13] S. Hayami, S. M. Holmes and M. A. Halcrow, *J. Mater. Chem. C*, **2015**, 3, 7775–7778.
[14] A. Bousseksou, G. Molnár, L. Salmon and W. Nicolazzi, *Chem. Soc. Rev.*, **2011**, 40, 3313.
[15] S. Brooker, *Chem. Soc. Rev.*, **2015**, 44, 2880–2892.
[16] P. Gütlich, *Struct. Bonding* **1981**, 44, 83–195
[17] P. Gütlich, A. Hauser, *Coord. Chem. Rev.* **1990**, 97, 1–22.
[18] O. Kahn, *Molecular Magnetism*, VCH, New York **1993**.
[19] G. A. Craig, O. Roubeau, G. Aromi, *Cordination Chemistry Reviews* **2014**, 269, 13–31.
[20] Z-Y. Li, H. Ohtsu, T. Kojima, J-W. Dai, T. Yoshida, B. K. breedloved, W-X. Zhang, H. Iguchi, O. sato, M. Kawano, M. Yamashita. *Angewadte Chemie International Edition* **2016**, 55, 5184–5189.
[21] T. Matsumoto, G. N. Newton, T. Shiga, S. Hayami, Y. Matsui, H. Okamoto, R. Kumai, Y. Murakani, H. Oshio, *Nature Communications* **2014**, 5:3865 doi: 10.1038/ncomms4865.
[22] E. A. Osorio, K. Moth-Poulsen, H. S. J. van der Zant, J. Paaske, P. Hedegård, K. Flensberg, J. Bendix,T. Bjørnholm, Nano Lett., **2010**, 10, 105–110.
[23] T. G. Gopakumar, F. Matino, H. Naggert, A. Bannwarth, F. Tuczek, R. Berndt, Angew. Chem., Int. Ed., **2012**, 51, 6262–6266.
[24] G. D. Harzmann, R. Frisenda, H. S. J. van der Zant, M. Mayor, Angew. Chem., Int. Ed., **2015**, 54, 13425–13430.
[25] N. Baadji, M. Piacenza, T. Tugsuz, F. D. Sala, G. Maruccio, S. Sanvito, Nat. Mater., **2009**, 8, 813–817.
[26] T. Miyamachi, M. Gruber, V. Davesne, M. Bowen, S. Boukari, L. Joly, F. Scheurer, G. Rogez, T. K. Yamada, P. Ohresser, E. Beaurepaire and W. Wulfhekel, Nat. Commun., **2012**, 3, 938.

View Article Online
DOI: 10.1039/C8DT01269E

[27] S. Sanvito, Chem. Soc. Rev., **2011**, 40, 3336.
[28] D. Aravena and E. Ruiz, J. Am. Chem. Soc., **2012**, 134, 777–779.
[29] P. N. Martinho, C. Rajnak, M. Ruben, *Nanoparticles, Thin Films and Surface Patterns from Spin-Crossover Materials and Electrical Spin State Control, in Spin-Crossover Materials: Properties and Applications* (ed. M. A. Halcrow), John Wiley & Sons Ltd, Oxford, UK. **2013**, 375–404.
[30] R. Frisenda, G. D. Harzmann, J. A. Celis Gil, J. M. Thijssen, M. Mayor, H. S. J. van der Zant, Nano Lett., **2016**, 16, 4733–4737.
[31] M. Bernien, H. Naggert, L. M. Arruda, L. Kipgen, F. Nickel, J. Miguel, C. F. Hermanns, A. Krüger, D. Krüger, E. Schierle, E. Weschke, F. Tuczek and W. Kuch, *ACS Nano*, **2015**, 9, 8960–8966.
[32] S. Hayami, Z. Gu, H. Yoshiki, A. Fujishima, O. Sato, *J. Am. Chem. Soc*., **2001**, 123, 11644–11650.
[33] J. Dugay, M. Aarts, M. Giménez-Marqués, T. Kozlova, H. W. Zandbergen, E. Coronado, H. S. J. van der Zant, *Nano Lett*., **2017**, 17, 186–193.
[34] K. Kumar, M. Ruben. *Coordination Chemistry Reviews* **2017**, 346, 176–20
[35] T. Buchen, P. P. Gütlich, K.H. Sugiyarto, H.A. Goodwin.*Chem. Eur. J.* 1996, 2, 1134–1138.
[36] G. Dupouy, M. Marchivie, S. Triki, J. Sala-Pala, J.Y. Salaum, C.J. Gomez-Garcia, P. Guionneau. *Inorg. Chem.*, **2008**, 47, 8921–8931.
[37] S. A. Barret, A. A. Kilner, M. A. Halcrow, *Dalton Trans.* **2011**, 40, 12021–12024.
[38] M. A. Halcrow, *Chem. Soc. Rev.* **2011**, 40, 4119–4142.
[39] S. Rodriguez-Fernandez, H. L. C. Feltham, S. Brooker, *Angewadte Chemie International Edition* **2016**, 55, 15067–15071.
[40] G. Aromi, C. M. Beavers, J. Sanchez Costa, G.A. craig, G. Minguez Esparllagas, A. Orera, O. Roubeau *Chemical Science* **2016**, 7, 2907–2915.
[41] D. Gentili, N. Demitri, B. Schafer, F. Liscio, I. Bergeti, G. Ruani, M. Ruben, M. Cavallini *Journal of Materials Chemistry* **2015**, 3, 7836–7844.
[42] K. H. Sugiyarto, H. A. Goodwin, *Chem. Phys. Letts*. **1987**, 139, 470–474.
[43] E. Coronado, M. C. Giménez-Lopez, C. Giménez-Saiz, J. M. Martínez-Agudo, F. M. Romero, *Polyhedron* **2003**, 22, 2375–2380.
[44] K. H. Sugiyarto, H. A. Goodwin, *Aust. J. Chem*. **1988**, 41, 1645–1663.
[45] K. H. Sugiyarto, D. C. Craig, A. D. Rae, H. A. Goodwin, *Aust. J. Chem*. **1994**, 47, 869–890.
[46] S. A. Barret, A. A. Kilner, M. A. Halcrow, *Dalton Trans.* **2011**, 40, 12021–12024.
[47] E. Coronado, J. C. Dias, M. C. Giménez-Lopez, C. Giménez-Saiz, C. Gómez-García, *J. Mol. Struct.* **2008**, 890, 215–220.
[48] E. Coronado, M. C. Giménez-Lopez, C. Giménez-Saiz, F. M. Romero, *CrystEngComm* **2009**, 11, 2198–2203.
[49] M. Clemente-León, E. Coronado, M. C. Giménez-López, F. M. Romero, S. Asthana, C. Desplanches, J-F. Létard, *Dalton Trans*. **2009**, 38, 8087–8095.
[50] M. C. Giménez-López, M. Clemente-León, E. Coronado, F. M. Romero, S. Shova, J. P. Tuchagues, *European Journal of Inorganic Chemistry* **2005**, 14, 2783–2787.
[51] M. Clemente-León, E. Coronado, M. C. Giménez-López, F. M. Romero, *Inorganic Chemistry* **2007**, 46, 11266–11276.
[52] M. A. Hoselton, L. J. Wilson, R. S. Drago, *J. Am. Chem. Soc.* **1975**, 97, 1722–1729.

View Article Online
DOI: 10.1039/C8DT01269E

[53] L. L. Martin, R. L. Martin, A. M. Sargeson, *Polyhedron* **1994**, 13, 1969–1980.
[54] R. Pritchard, C. A. Kilner and M. A. Halcrow, *Chem. Commun.* **2007**, 577, 579–577.
[55] J. A. Broomhead, *Aust. J. Chem.* **1962**, 15, 228–230.
[56] Y. Lin, S. A. Lamg, *J. Heterocycl. Chem.* **1977**, 14, 3454–3457.
[57] H. Arend, J. J. Connelly, *Journal of Crystals Growth*, **1982**, 56, 642–644.
[58] G.A. Bain, J.F. Berry. *J. Chem Educ.* 2008, 85, 532–536.
[59] Z. Otwinowski, W. Minor, DENZO-SCALEPACK, Processing of X-ray Diffraction Data Collected in Oscillation Mode. In Methods in Enzymology, Volume 276, Macromolecular Crystallography, part A; Carter, C. W., Jr., Sweet, R. M., Eds.; Academic Press: New York, **1997**, 307-326.
[60] A. Altomare, M. C. Burla, M. Camalli, G. Cascarano, C. Giacovazzo, A. Guagliardi, A. G. G. Moliterni, G. Polidori, R. Spagna, *J. Appl. Crystallogr*. **1999**, 32, 115–119.
[61] L. J. Farrugia, *J. Appl. Crystallogr.* **1999,** *32,* 837–838.
[62] G. M. Sheldrick, *SHELXL-97, Program for the refinement of crystal structures from diffraction data,* University of Göttingen, Göttingen,Germany, **1997.**
[63] R.H. Blessing *J. Appl. Cryst*. **1997**, *30*, 421-426.
[64] K. H. Sugiyarto, W. A. McHale, D. C. Craig, A. D. Rae, H. A. Goodwin, Dalton Trans., **2003**, 2443.
[65] T. D. Roberts, F. Tuna, T. L. Malkin, C. A. Kilner, M. A. Halcrow, Chem. Sci. **2012**, 3, 349–354.
[66] K. H. Sugiyarto, W-A. McHale, D. C. Craig, A. D. Rae, M. L. Scudder, H. A. Goodwin, *Dalton Trans*. **2003**, 22, 2443–2448.

View Article Online
DOI: 10.1039/C8DT01269E

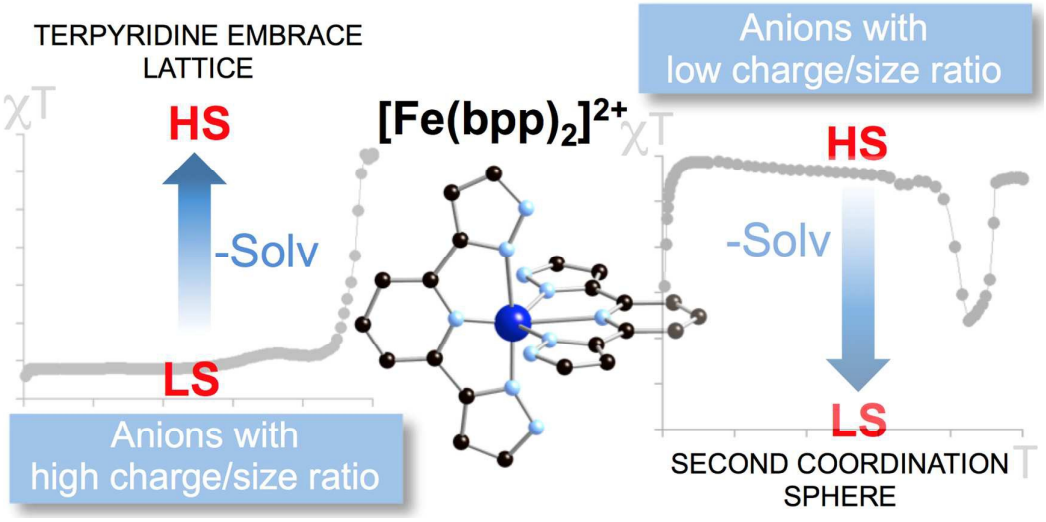

Revealing the reasons why the lattice-solvent stabilise one spin form over the other in $[Fe(bpp)_2]^{2+}$ complexes bearing anions with different charge/size ratio.